Automated Detection of Pulmonary Nodules from Whole Lung Helical CT Scans: Performance comparison for isolated and attached nodules

Andinet A. Enquobahrie[a] and Anthony P. Reeves[a] and

David F. Yankelevitz[b] and Claudia I. Henschke[b]

[a]School of Electrical and Computer Engineering, Cornell University, Ithaca, NY
[b]Department of Radiology, Weill Medical College of Cornell University, New York, NY

ABSTRACT

The objective of this research is to evaluate and compare the performance of our automated detection algorithm on isolated and attached nodules in whole lung CT scans. Isolated nodules are surrounded by the lung parenchyma with no attachment to large solid structures such as the chest wall or mediastinum surface, while attached nodules are adjacent to these structures. The detection algorithm involves three major stages. First, the region of the image space where pulmonary nodules are to be found is identified. This involves segmenting the lung region and generating the pleural surface. In the second stage, which is the hypothesis generation stage, nodule candidate locations are identified and their sizes are estimated. The nodule candidates are successively refined in the third stage a sequence of filters of increasing complexity.

The algorithm was tested on a dataset containing 250 low-dose whole lung CT scans with 2.5mm slice thickness. The dataset was partitioned into 200 and 50 scans for training and testing the algorithm. Only solid nodules were considered in this study. Experienced chest radiologists identified a total of 447 solid nodules. 345 and 102 of the nodules were from the training and testing datasets respectively. 126(28.2%) of the nodules in the dataset were attached nodules.

The detection performance was then evaluated separately for isolated and attached nodule types considering different size ranges. For nodules 3mm and larger, the algorithm achieved a sensitivity of 97.8% with 2.0 false positives (FPs) per scan and 95.7% with 19.3 FPs per scan for isolated and attached nodules respectively. For nodules 4mm and larger, a sensitivity of 96.6% with 1.5 FP per scan and a 100% sensitivity with 13 FPs per scan were obtained for isolated and attached nodule types respectively. The results show that our algorithm detects isolated and attached nodules with comparable sensitivity but differing number of false positives per scan. The high number of false positives for attached nodule detection was mainly due to the complexity of the mediastinum lung surface.

Keywords: Computer aided detection, Pulmonary nodules, FROC, Segmentation, Hypothesis generation

1. INTRODUCTION

Lung cancer is the leading cause of cancer death in the United States. According to the American Cancer Society,[1] there will be approximately 171,900 new cases of lung cancer in the United States: 91,800 among men and 80,100 among women in the year 2003. About 157,200 lung cancer deaths are predicted for the same year.[1] Although five years survival of lung cancer is only 14%, results from the ELCAP project[2] shows that detection and treatment of lung cancer at early stages may result in substantially higher overall cure rate. Hence, lung cancer screening has recently received considerable attention.

In the lung cancer screening process, radiologists analyze CT images of asymptomatic patients searching for nodules. Henschke et al[3] reported that use of low-dose CT as compared to chest radiography as the initial screening test resulted in the detection of substantially greater proportion of small early stage cancers. CT scanners

Corresponding Author: Andinet A. Enquobahrie: andy@ece.cornell.edu, Telephone: 607-255-0963; School of Electrical and Computer Engineering, Cornell University, 357 Rhodes Hall, Ithaca 14850, NY, USA

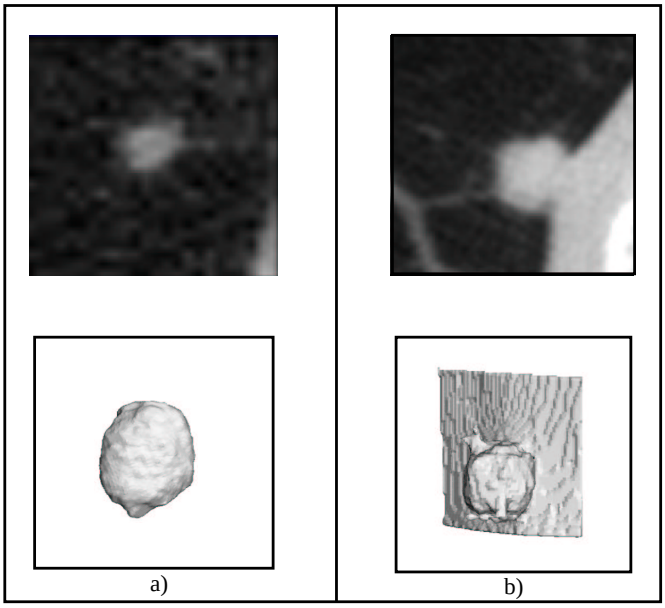

Figure 1. Pulmonary nodule types: A 2D slice and 3D rendered images a) Isolated Nodule b) A nodule attached to pleural surface

produce many thin slice axial images per patient. Radiologists are then confronted with the overwhelming task of interpreting a massive quantity of images. This has necessitated the development of a computer aided diagnosis (CAD) system. CAD consists of three stages: nodule detection, characterization, and disease assessment. The efficacy of the entire CAD system is highly dependent on the reliability and robustness of the nodule detection stage.

Solid pulmonary nodules can be broadly classified into two groups: isolated and attached nodules. Isolated nodules have no attachments to a large solid structure and are surrounded by lung parenchyma. These nodules have, in general, a spherical shape. However, the spherical shape may be distorted by other small lung structures such as vessels, bronchi, scars and regions of morbidity. An example of an isolated nodule is shown in Figure 1a. The second group consists of nodules attached to large dense structures, an example of which is shown in Figure 1b. Nodules attached to the pleural surface are the most prevalent of this type.

Most of the research done on automated nodule detection has targeted only isolated nodules. Fan et al[4] implemented an adaptive 3D region growing algorithm followed by a classification scheme that makes use of geometric features such as diameter, volume, sphericity, mean intensity value and standard deviation of intensity. This algorithm only detects nodules with very small vasculature connections and no large solid structure attachment. Taguchi et al[5] used morphological analysis techniques to detect suspicious regions. Penedo et al[6] developed a computer aided detection system based on a two level artificial neural network. The first network performs detection of suspicious regions, while the second one classifies the regions based on the curvature peak on all points in the suspicious region. They reported 89% - 96% sensitivity with 5-7 FPs per slice. Artificial neural networks' capabilities have also been used by Lo et al.[7] Object-based deformation techniques have been incorporated into detection systems. Lou et al[8] used deformation techniques to differentiate lung nodules from blood vessels in their 3D CT lung nodule detection system. This research did not address surface irregularities that occur in nodules with significant vasculature connections. Knowledge based techniques have also been used in research work done by Erberich et al[9] and Brown et al.[10]

Only a few researchers have developed automated techniques for detection of both isolated and attached nodules. Aramato et al[11] implemented a computerized scheme that used 2D and 3D extracted features for isolated nodule detection and a rolling ball algorithm for attached nodule detection. In the rolling ball algorithm,

a circle is moved along the lung contour searching for indentations. Lung border pixel locations where the ball touches more than one pixel are marked as potential nodule locations. A sensitivity of 85% and specificity of 89% was reported indicating an overall sensitivity of 70% with an average of three FPs per slice. However, neither the total number of attached (pleural) nodules in the nodule database nor the detection performance for this type of nodule were reported separately. Lee et al[12] used a template matching technique based on a genetic algorithm to detect nodules. Different were generated for nodules with and without an attachment to the chest wall. Circular and semicircular templates with Gaussian distribution were used to detect isolated and attached nodules respectively. The semicircular template were oriented in the direction of the boundary normal to detect pleural nodules. They reported 72.0% sensitivity with 4.4 FPs per slice and 70.8% sensitivity with 0.5 FPs per slice for isolated and attached nodule types , respectively. Although, they developed an elegant mathematical model of a nodule, the algorithm resulted in a very high number of false positives. Gurcan et al[13] used a k-means clustering technique for nodule candidates generation and 2D/3D features to reduce the number of false positives. In addition, they introduced a a new indentation detection technique for pleural nodule detection. In this technique, for every pair of lung contour points, they calculated the Euclidean distance and the distance along the lung contour in clockwise and counterclockwise directions between the two points. The three distance metrics were used to define a feature, then used by rule based classifier. Only five pleural nodules were available in their database. Curvature techniques were explored by Kanazawa et al[14] for irregularity detection in the lung boundaries. Parts of the contour with rapid curvature change were marked as suspicious indentations.

In all of the above research, there are two aspects in which attached nodules have not received as much treatment as isolated nodules. First, with the exception of Lee et al,[12] the algorithm performance for the detection of attached nodules was not evaluated and reported separately. A separate evaluation would be necessary since a different algorithm was implemented or a different set of feature metrics would be used to detect attached nodules. Secondly, attached nodules that are not attached to the chest wall have not been explored. In our database, in addition to the nodules attached to the chest wall, there are several attached nodules in the lower part of the lung (near the diaphragm) and in the hilar region.

In this study, we developed a CAD system for the detection of both attached and isolated nodules types with high sensitivity and low number of false-positives per case. The algorithm was tested on a dataset with a larger number of both isolated and attached nodules compared to previous studies. The performance of the detection system for the two types of nodule was compared.

2. METHODS

A multi-stage detection algorithm was developed to automatically detect pulmonary nodules from whole lung CT scans. The algorithm flowchart is shown in Figure 2. The algorithm has three major stages.

First, the region of the image space where pulmonary nodules may be located is identified. This involves segmenting the lung region and generating the pleural surface. An axial slice image and its corresponding segmented regions are shown in Figure 3. The lung region and the pleural surface represent the 3D search space for isolated and attached nodules respectively. The lung region segmentation algorithm consists of creating a mask representing the lung volume and applying a logical AND operation between the mask and the original image. For the pleural surface generation, the boundary of the segmented lung region is first traced. The boundary pixels are then connected and labeled to form a 3D search space.

The second stage is the hypothesis generation stage where nodule candidate locations are identified and their sizes are estimated. For isolated nodules, this involves identifying 3D connected regions which satisfy solid center and limited distance criteria. For attached nodules, candidates are generated by analyzing first the surface morphology and then the volume occupancy characteristics curve of suspicious surface voxels. Suspicious surface voxels are generated by comparing the surface before and after morphological closing operation. This operation is demonstrated in Figure 4. The suspicious surface voxels are further refined by analyzing their volume occupancy distribution curve. Volume occupancy, at a particular surface voxel is defined as the ratio of the number of lung parenchyma voxels within a template of a certain size to the volume of the template. The volume occupancy calculation is repeated for incrementally increasing size templates and the distribution is plotted. Surface voxels with a distinct peak in the distribution curve are marked as attached nodule candidates. Surface voxels belonging

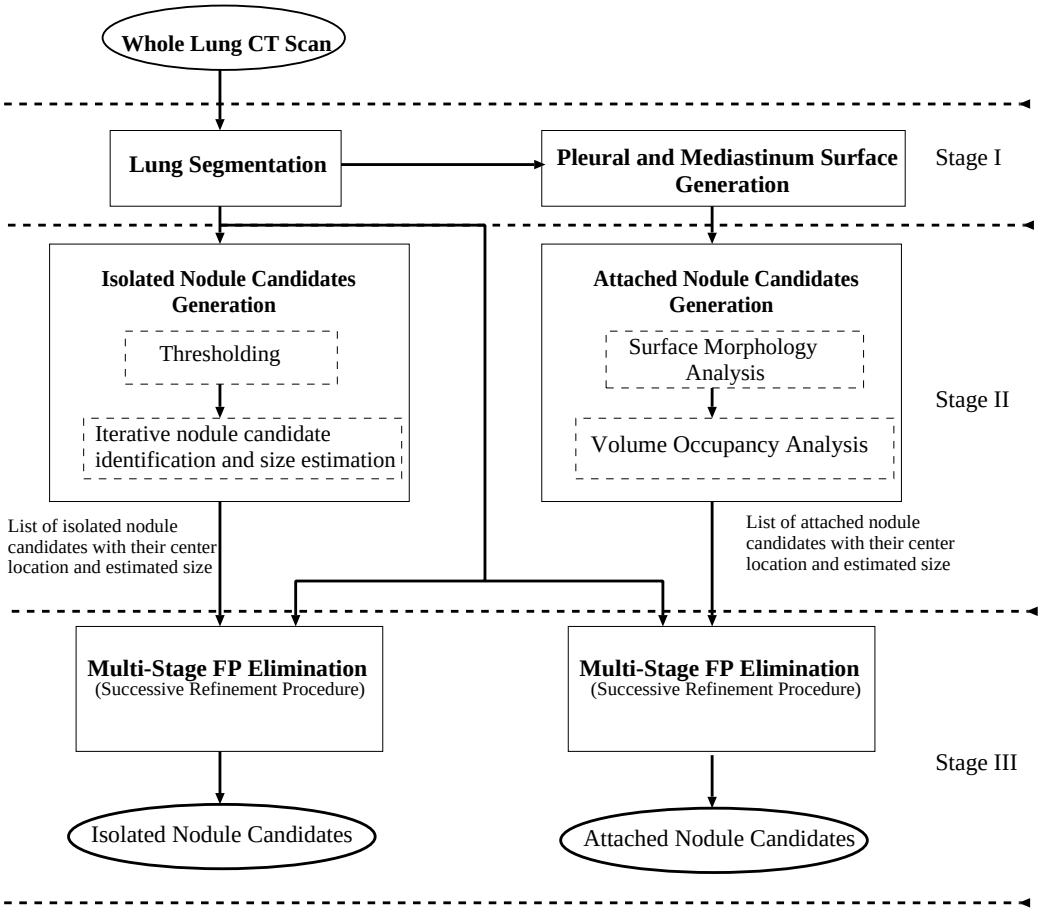

Figure 2. Detection Algorithm Flowchart

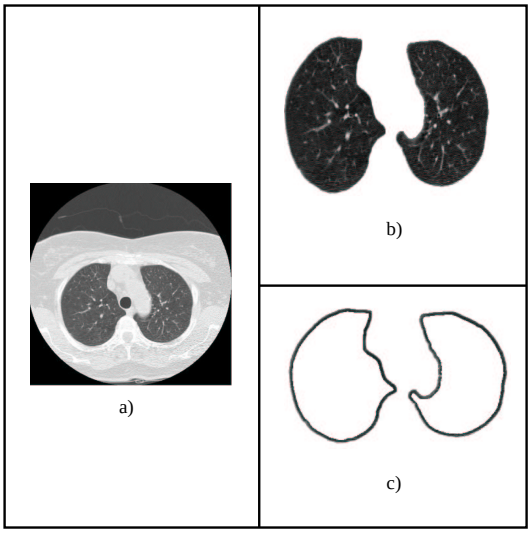

Figure 3. A single axial image and the corresponding segmented regions for nodule detection: a) Original scan b) Lung parenchyma c) Pleural surface

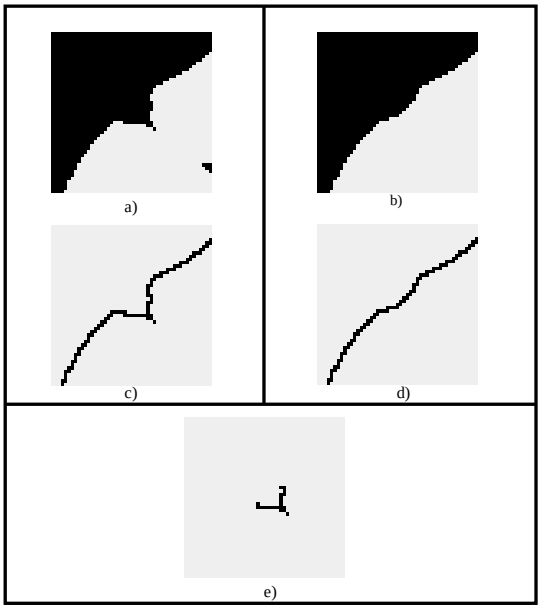

Figure 4. Morphological analysis method to identify suspicious surface voxels : a) Segmented lung parenchyma b) Lung parenchyma after morphological closing operation c) and d) surface voxels before and after morphological closing operation respectively. e) Difference image between c) and d)

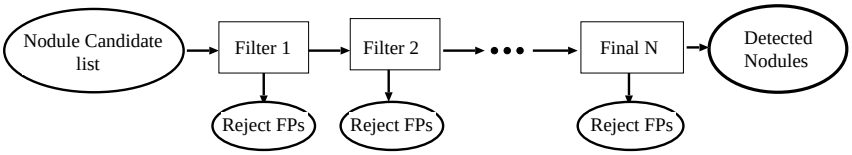

Figure 5. Multi-stage successive nodule candidate refinement

to the same nodule candidate are clustered together to ensure a single response for a single nodule candidate. Several heuristics have been incorporated to make the algorithm more efficient.

Finally, in the third stage, the nodule candidates are successively refined using a sequence of filters of increasing complexity. A multi-stage filtering procedure, illustrated in Figure 5, is used for this purpose. This approach is effective in minimizing the computation time without sacrificing performance. The first two filters remove vessels and vessel bifurcation points from the nodule candidate list. These filters are based on an analysis of the nodule candidate's attachment surface area to other structures at original and resampled isotropic resolution (see Figure 6). A large percentage of false positives are eliminated by these filters. The nodule candidate list is then further refined using 3D moment-based and spherical-model filters.

3. DATABASE

Our current dataset consists of 250 low-dose whole lung CT scans. We partitioned the dataset into 200 training and 50 testing cases. The CT scans were acquired using a GE LightSpeed helical scanner (KVP=140, mA=40). The average number of slices per scan is 126. The resolution of the images in the x-y plane ranges from 0.5 to 0.7 mm/pixel, with a slice thickness of 2.5mm. A total of 447 nodules were identified by two experienced chest radiologists. These nodules were used as a gold standard to evaluate the accuracy of our detection algorithm. The classification of identified nodules based on size and shape (whether it is isolated or attached) is shown in Table 1. In the nodule dataset, 345 (77.2%) and 102 (22.8%) of the nodules were from the training and

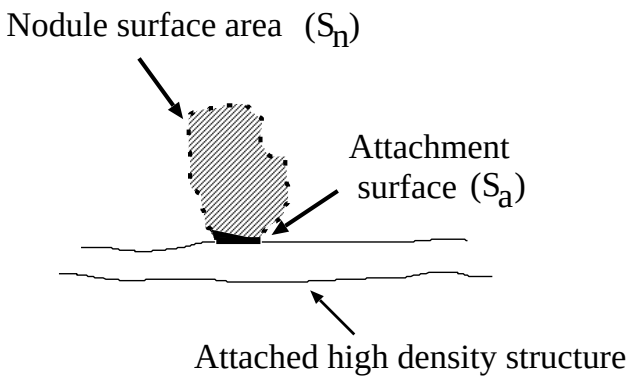

Figure 6. Nodule candidate attachment analysis

Table 1. Nodule size and type distribution for training and testing datasets

			Dataset Type	
			Training	Testing
Number of Cases			200	50
Type of Nodules	Isolated	$<= 2mm$	119	30
		$3-4mm$	90	25
		$>= 5mm$	37	20
		$Total$	246	75
	Attached	$<= 2mm$	37	4
		$3-4mm$	38	14
		$>= 5mm$	24	9
		$Total$	99	27
Total Number of Nodules			345	102

testing databases respectively. Attached nodules make up 126 (28.2%) of the nodules in the dataset. The nodule database contains 190 (42.5%) $\leq 2mm$, 167 (37.3%) $3-4mm$ and 90 (20.2%) $\geq 5mm$ nodules.

4. RESULTS

The algorithm performance was evaluated for isolated and attached nodule types separately. In addition, the performance was compared for different nodule size ranges. The free response receiver operating characteristics (FROC) curves are shown for both types of nodules in Figure 7. In these graphs, the detection performance was plotted for different size ranges (Nodule size $\geq$ d). The results show clearly the dependence of the algorithm performance on nodule type and size range. The algorithm achieved better performance for isolated nodules compared to attached nodules. In addition, for both nodule types, the larger the nodule size range, the better the performance obtained.

For nodules 3mm and larger, the algorithm achieved a sensitivity of 97.8% with 2.0 false positives per scan and 95.7% with 19.3 false positives per scan for isolated and attached nodules respectively. For nodules 4mm and larger, a sensitivity of 96.6% with 1.5 false positives per scan and a sensitivity of 100% with 13 false positives per scan were obtained for isolated and attached nodule types respectively.

5. DISCUSSION

We identified several challenging cases in our study. Selected cases of isolated and attached nodule types are shown in Figure 8 and 9 respectively. We observed two main types of false positives in our study: small vessel

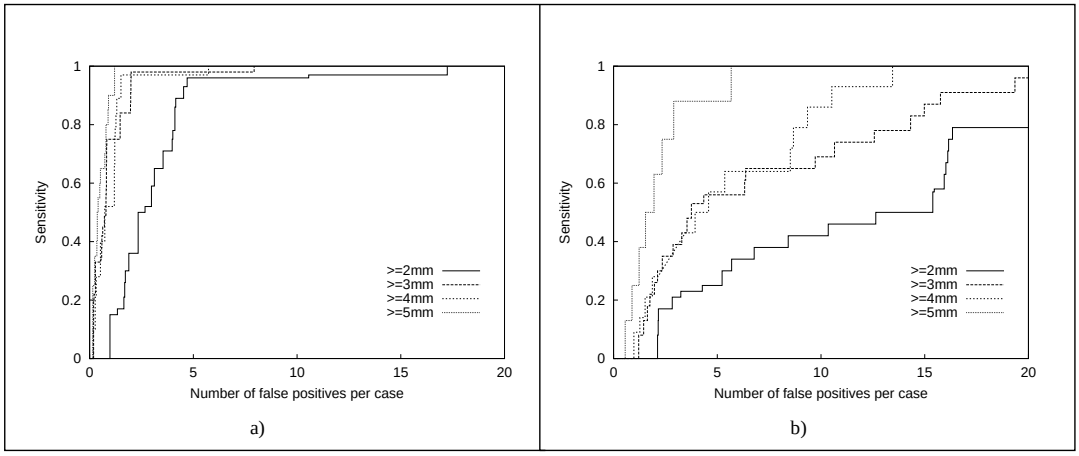

Figure 7. a) Isolated and b) Attached nodules detection FROC curve

bifurcation points and pericardium ridges. Small vessel bifurcation points (Figure 10a) appear as isolated nodules due to partial voxel effects. This is mainly due to the thick slice thickness scans used to test the algorithm. For the attached nodule types, pericardial ridges are typically detected as small mediastinum nodules. A sample case is shown in Figure 10b. Other false positives include hilar vessels and bronchial wall thickening.

6. CONCLUSION

We developed a multi-stage detection algorithm for both isolated and attached nodule types. We introduced a successive false positive elimination approach which is computationally efficient and is extensible to include more complex filters. The algorithm was tested on a large dataset built from a screening study. The results show that our technique detects isolated and attached nodules with comparable sensitivity but differing number of false positives per scan. The high number of false positives for attached nodule detection was mainly due to the complexity of the mediastinum surface region. Future work will mainly concentrate on two tasks. First, we will attempt to further reduce the attached nodule false positives by adding more model-based filters to the filter cascade. Second, we will test the algorithm on thinner slice CT scans.

REFERENCES

1. A. C. Society, *Cancer Facts and Figures 2003*, Atlanta, 2003.
2. C. I. Henschke, D. I. McCauley, D. F. Yankelevitz, D. P. Naidich, G. McGuinness, O. S.Miettinen, D. M. Libby, M. W. Pasmantier, J. Koizumi, N. K. Altorki, and J. P. Smith, "Early lung cancer action project : Overall design and findings from baseline screening," *Lancet* **354**, pp. 99–105, 1999.
3. C. I. Henschke, D. P. Naidich, D. F. Yankelevitz, G. McGuinness, D. I. McCauley, J. P. Smith, D. M. Libby, and M. W. Pasmantier, "Early lung cancer action project : Initial findings on repeat screening," *Cancer* **92**, pp. 153–159, 2001.
4. L. Fan, C. Novak, G. K. J. Qian, and D. Naidich, "Automatic detection of lung nodules from multi-slice low-dose CT images," *Proc. SPIE* **4322**, pp. 1828–1835, 2001.
5. H.Taguchi, Y.Kawata, N. Niki, H.Satoh, H.Ohmatsu, K.Eguchi, M.Kaneko, and N. Moriyama, "Lung cancer detection based on helical CT images using curved surface morphology analysis," *Proc. SPIE* **3661**, pp. 1307–1313, 1999.
6. M.G.Penedo, M.J.Carreira, A.Mosquera, and D. Cabello, "Computer-aided diagnosis: a neural-network based approach to lung nodule detection," *IEEE Transactions on Medical Imaging* **17(6)**, pp. 872–879, 1998.

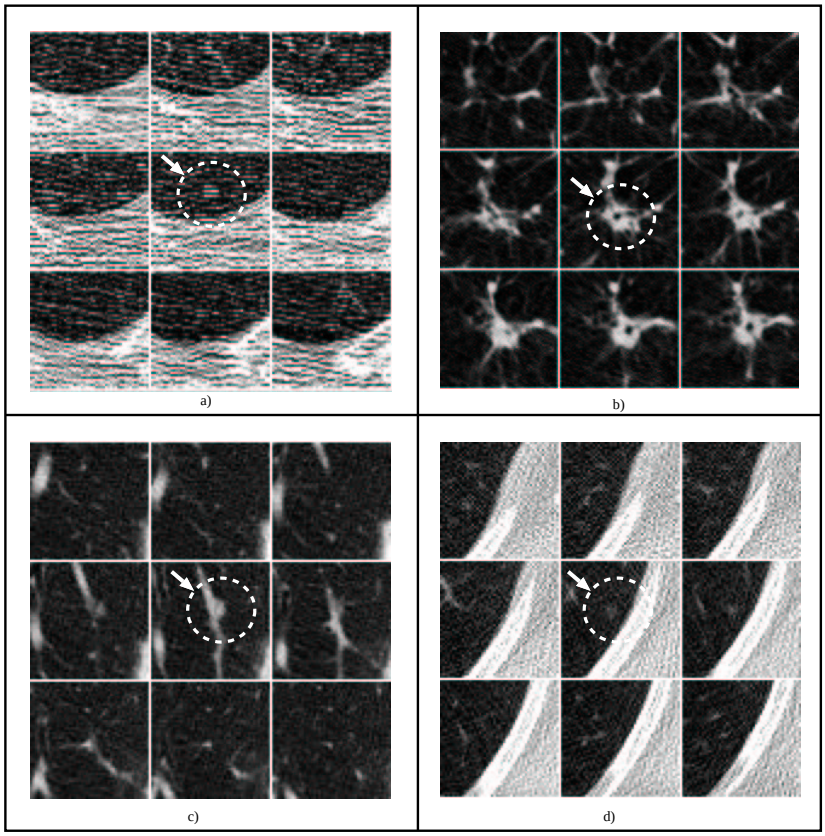

Figure 8. Image montage of challenging isolated nodule cases: a) A small nodule in apical portion of the lung with a large amount of noise. b) A nodule with a bronchus passing through it. c) A small nodule abutting a vessel. d) A faint (low intensity) nodule.

7. S-CB.Lo, S.-L. A. Lou, J.-S. Lin, M. Freedman, M. V. Chien, and S. K. Mun, "Artifical convolution neural network techniques and applications for lung nodule detection," *IEEE Transactions on Medical Imaging* **14(4)**, pp. 711–718, 1995.
8. S. Lou, C. Chang, K. Lin, and T. Chen, "Object based deformation technique for 3-d CT lung nodule detection," *Proc. SPIE* **3661**, pp. 1544–1552, 1999.
9. S. Erberich, K. Song, H.Arakawa, H. K. Huang, R. Webb, K. S. Hoo, and B. Loo, "knowledge-based lung nodule detection from helical CT," *RSNA 1997 Annual Meeting*, 1997.
10. M. Brown and M. F. McNitt-Gray, "Method for segmenting chest CT image data using an anatomical model: preliminary results," *Proc. SPIE* **16**, pp. 828–839, 1997.
11. S. Armato, M. L. Giger, C. J. Moran, J. Blackburn, K. Doi, and H. MacMahon, "Computerized detection of pulmonary nodules on CT scans," *RadioGraphics* **19**, pp. 1303–1311, 1999.
12. Y.Lee, T. Hara, H. Fujita, S. Itoh, and T. Ishigaki, "Automated detection of pulmonary nodules in helical CT images based on an improved template-matching technique," *IEEE Transactions on Medical Imaging* **20**, pp. 595–604, 2001.
13. M. N. Gurcan, B. Sahiner, N. Petrick, and H.-P. Chan, "Lung nodule detection on thoracic computed tomography images: Preliminary evaluation of a computer-aided diagnosis system," *Medical Physics* **29**, pp. 2552–2558, November 2002.
14. K.Kanazawa, M.kubo, N.Niki, H.Satoh, H.Ohmatsu, K.Eguchi, and N.Moriyama, "Computer assisted diagnosis of lung cancer using helical x-ray CT," *Proc. SPIE*, pp. 381–385, 1996.

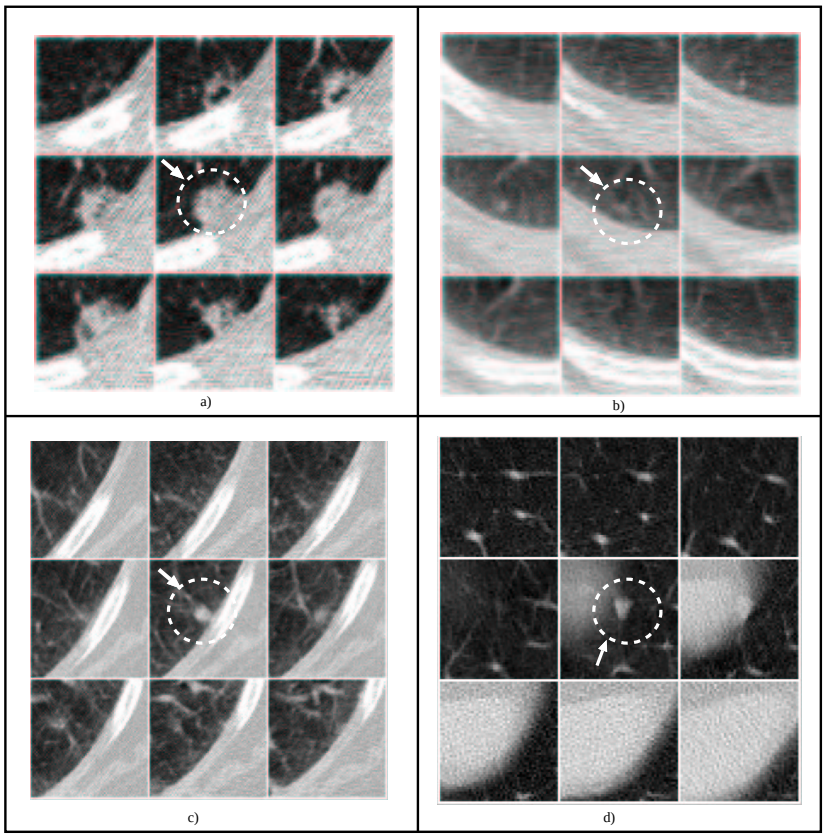

Figure 9. Image montage of challenging attached nodule cases: a) A pleural nodule with cystic spaces. b) A small pleural nodule in a noisy scan. c) A pleural nodule with vessel attachments. d) A nodule on the convex diaphragmatic surface, that is obscured by partial volume effects.

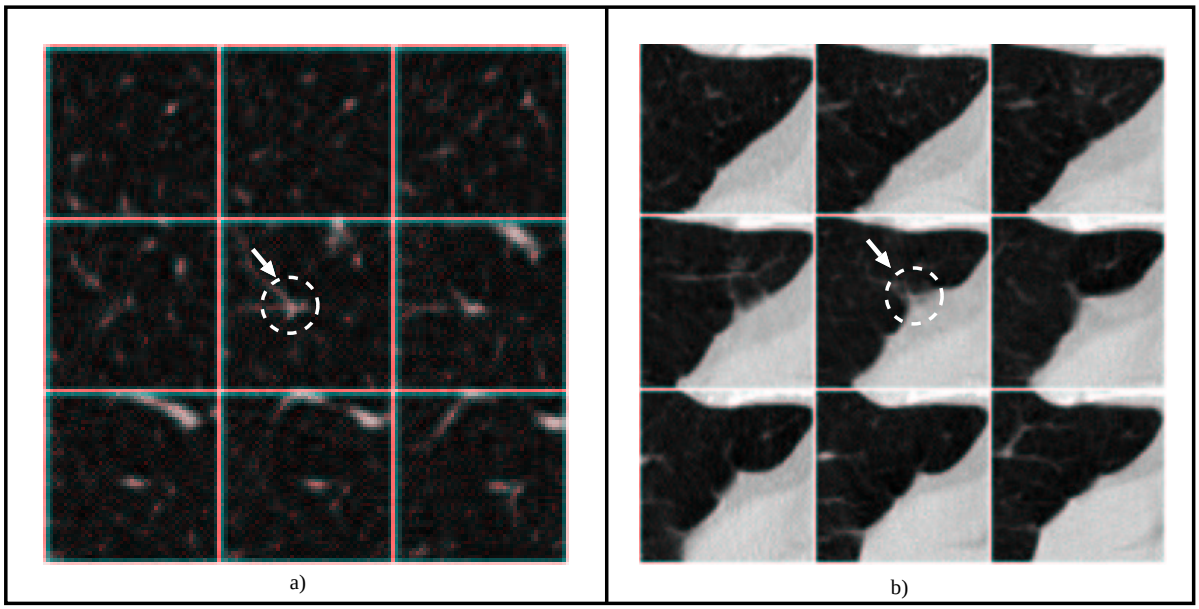

Figure 10. Image montages of typical false positives: a) A small vessel bifurcation point b) Pericardial ridge